J Mater Sci (2009) 44:2513–2519
DOI 10.1007/s10853-009-3325-y

The real part of AC conductance in amorphous nanocomposites ferromagnetic alloy–dielectric

A. M. Saad

Received: 18 August 2008 / Accepted: 6 February 2009 / Published online: 5 March 2009

Abstract Results of AC conductivity of the granular nanocomposites consisting of amorphous ferromagnetic alloy nanoparticles ($Fe_{0.45}Co_{0.45}Zr_{0.10}$) embedded into amorphous dielectric matrix (Al_2O_3) are presented and analyzed here. Conductivity measurements were made for the samples of different metal-to-dielectric ratio x ($25 < x < 65$ at.%) in the frequency range of 0.1–1000 kHz at temperature of 80–340 K. Real part of AC conductance at low frequencies ($f \leq 5$ kHz) have shown temperature dependencies $\sigma_{real}(T)$ corresponding to Mott hopping regime at x below the percolation threshold and metallic one beyond the percolation threshold. It was shown that $\sigma_{real}(T)$ dependencies satisfactorily follow the known relations of 3D percolate models with critical indexes $t \approx 1.6, q \approx 0.9$, and $s = 0.62$. The numerical estimations of the density of localized states $N(E_F)$ displayed a tendency to be decreased with x increase and the electron wave-function localization length a was about 11 nm.

Introduction

Granular nanocomposites FeCo-based ferromagnetic alloy–amorphous dielectric matrix has a special place among nanostructured materials. Though looking homogeneous on the macroscopic scale, such binary composite systems are disordered and inhomogeneous on the nanoscale. The important applications of these systems are the conductive adhesives, protection layers against electromagnetic radiation, and novel electronic and magnetoelectronic devices based on size effects like the single electron tunneling [1]. Depending on the metallic phase concentration x, the electrical properties of such mixtures can vary between those of the matrix and of the filler. The typical binary composite material has a critical concentration, percolation threshold x_C [2], approached when a continuous cluster of filler particles is formed through the sample.

The low-frequency impedance measurements in the typical frequency range of $10^2 < f < 10^6$ Hz are valuable and supplied additional information on the conductivity mechanisms that DC conductance measurements alone did not provide [3–5], i.e., this technique has been used extensively by many researchers [6–11] for the disordered and inhomogeneous materials. These measurements along with the DC conductance provided important information about the carrier transport mechanisms and magnetic state of the nanocomposites versus composition, conditions of preparation, temperature, external electric and magnetic fields, etc.

The granular composite materials, which consist of FeCo-containing soft ferromagnetic nanoparticles embedded into the dielectric matrix, were given a great interest and considered as nearly ideal core materials for many of high-frequency applications [8–11]. Their low coercivity along with high saturation magnetization, high in-plane anisotropy field, and high resistivity are beneficial to obtain high power density and low power loss in different applications. Also such nanocomposites can be promising as memory media with super-high density of magnetic recording ability used in magnetic recording heads, RF and SHF shielding, etc. Recently an increased interest has been demonstrated in such nanogranular systems due to the observed GMR/TMR effects [12–20]. Note also that most of the electrical, magnetic, and other properties of FeCo-containing nanocomposites vary drastically with the external conditions just near the percolation threshold x_C [11, 21–24]. These make

A. M. Saad (✉)
Al-Balqa Applied University, Salt-Jordan,
P.O. Box 4545, Amman 11953, Jordan
e-mail: daas005@yahoo.co.uk; fedotov@bsu.by

the nanocomposites very attractive for the construction of various kinds of sensors, actuators, detectors, etc.

The carrier transport analysis of FeCo-containing nanogranular composite films, earlier evaluated from small-signal DC and low-frequency AC measurements, has shown a high-resistive state far before the percolation threshold and the low-resistive behavior beyond x_C [11, 22–24]. These measurements have also revealed a strong influence of the films preparation conditions (especially, substrates temperature during deposition) on their electro-magnetic properties and position of the percolation threshold [11, 22, 24].

As was mentioned above, the impedance spectroscopy, the frequency response of the electrical properties, along with DC conductance provided important information about the carrier transport regimes in the nanocomposites metal-insulator versus composition, conditions of preparation, temperature, external electric and magnetic fields, etc. [25, 26]. So the goal of this paper is to study the real part of AC conductance of the composites, consisting of alloy ferromagnetic nanoparticles ($Fe_{0.45}Co_{0.45}Zr_{0.10}$) embedded into a non-magnetic amorphous dielectric matrix (Al_2O_3), for different volume concentrations of metallic nanoparticles and compare it with their DC behavior.

Experimental

The studied 3–5 μm thick films $(Fe_{0.45}Co_{0.45}Zr_{0.10})_x(Al_2O_3)_{1-x}$ with $25 < x < 65$ at.% were deposited using the ion-beam sputtering of the compound target onto the motionless substrate with argon gas in the chamber. Contrary to the previous samples preparation described in our previous works [22–24], the substrate here during sputtering was not water-cooled and its temperature was about 100 °C. The original configuration of the compound target enabled one to prepare composite films with the different metallic-to-dielectric fraction x in one technological process [21].

The structure of the as-deposited film composites was investigated using transmission (TEM), scanning (SEM) electron microscopes, and X-ray diffraction (XRD) measurements. TEM microscopy of some of the thin films confirmed their granular structure with dimensions of metallic nanoparticles of 2–10 nm embedded into amorphous alumina (Fig. 1a). SEM microscopy of the films showed their cellular structure (Fig. 1b) as that for the samples deposited at lower temperatures (see [22]) but with smaller cells which were lesser scattered by dimensions (100–200 nm as compared to 100–400 nm in [22]).

Content measurements of the chemical elements constitute the composites were made using a special microprobe X-Ray analysis in LEO 1455VP.

Magnetic and valence states of Fe ions in the composites for different metal-to-dielectric ratios were studied using Mössbauer spectroscopy. Mössbauer spectra were recorded in transmission geometry at room temperature using MS2000 spectrometer with ^{57}Fe/Rh source and $YAlO_3$:Ce crystalline scintillation detector [27].

AC conductance measurements were made for the rectangular shape (10×2 mm^2) samples. Impedance parameters of the composites were measured at 30 frequencies between 100 Hz and 1 MHz using the precision LCR-meter HP 4284A in the temperature range of 80–340 K with the temperature change rate of 0.5 K/min. The temperature in the measurement chamber was controlled within the accuracy of 1×10^{-3} K and thicknesses of the films were determined from their cross section using SEM measurements.

Results and discussion

The behavior of AC conductance in composite materials is strongly dependent on sample concentration relative to the percolation threshold x_C, metallic-to-dielectric phases conductance ratio R_m/R_d, geometric parameters of metallic nanoparticles, and also characteristics of dielectric strata (dimensions, shape, topology, density of localized states, etc.) [28]. In accordance with the latest models of the percolation theory, for high difference in conductance of several orders of magnitude between metallic and dielectric phases and the metallic component concentrations below the percolation threshold ($x < x_C$), a continuous conducting-current (percolating) cluster did not form and the carrier transport was carried out mainly through the dielectric strata between the metallic nanoparticles. However, beyond the

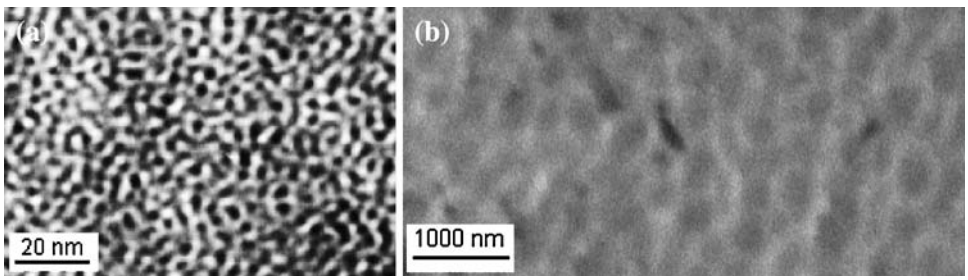

Fig. 1 TEM (**a**) and SEM (**b**) images of the films with $x = 31$ at.%

percolation threshold ($x > x_C$) metallic nanoparticles formed continuous conducting-current clusters, parts of their skeleton shunting any dielectric strata, with the composite shifting to the metallic side of the metal-insulator transition (MIT).

A short review of our earlier results can be made, before describing the AC conductance measurements, using structural and DC conductance properties of the nanocomposite films deposited on water-cooled substrate (approximately at 10–15 °C). TEM microscopy of the as-deposited films revealed that their granular structure was made of amorphous $Co_{0.45}Fe_{0.45}Zr_{0.10}$ alloy nanoparticles of 6–10 nm dimensions randomly distributed in amorphous alumina matrix [11]. Comparing the SEM, XRD, and Mössbauer data [7, 9] of the samples concluded that the bcc-FeCo was a dominating phase formed in the studied nanocomposite films.

The combined investigations of the Mossbauer spectra, magnetization, and DC/AC conductance of the composites sputtered on water-cooled substrate revealed that their magnetic state and behavior of conductance was strongly dependent on relative content of the metallic phase [21–24, 27]. In particular, before the percolation threshold ($x < x_C \approx$ 45–47 at.%) the nanocomposites were in a superparamagnetic state but beyond x_C they were in a ferromagnetic state. Moreover, the mechanism of electron transport in the films changed from hopping of electrons by localized states in the dielectric Al_2O_3 matrix to metallic regime when crossing the percolation threshold x_C.

The dependences of room temperature AC conductance σ at low frequencies ($f \leq 5$ kHz) on volume concentration x of metallic phase for the films studied in this paper (sputtered on non-water-cooled substrate) are shown in Fig. 2a on curve 1. As is seen, this curve looks very similar to that observed for the DC conductance measured earlier (compare with curve 1 in Fig. 1 in [24]) showing the increase of films conductivity as the metallic phase content increases in the studied region of x.

Vacuum annealing of the samples at low-temperature (650 K) and for a short time (30 min) resulted in evident changes in the $\sigma(x)$ dependence (see, curve 2 in Fig. 2a). The used heat treatment procedure allowed to determine the percolation threshold accurately in accordance with the method described in [29]. Accordingly this method position of x_C, defined by the intersection point of the curves 1 and 2 in Fig. 2a, is ≈42 at.% (a little lower than the value observed in [22, 24–27]).

In order to check the percolation models application for the studied composites the analysis of the $\sigma(x)$ dependence for the as-deposited films were made in more details around the percolation threshold by rebuilding of curve 1 in Fig. 2a in double logarithmic coordinates $\lg(\sigma)$ vs. $\lg|x - x_C|$ (see curves 1 and 2 in Fig. 2b) where x_C was 42 at.%.

According to the percolative models [2, 30] for the binary mixture of particles with infinite resistance (ideal insulator) and highly conductive particles (metallic) for $x < x_C$ the effective conductance $\sigma(x) = 0$ while for $x > x_C$ it follows the relationship of

$$\sigma(x) = \sigma_m(x - x_C)^t \quad (1)$$

where σ_m is conductivity of the metallic phase at $x = 1$ and t is critical index. The value of $\sigma(x = x_C)$ for the percolative model is related to the conductivities of metallic σ_m and dielectric σ_d phases by

$$\sigma(x_C) = \sigma_m\left(\frac{\sigma_d}{\sigma_m}\right)^s \quad (2)$$

where s is critical index. If $\sigma(x_C) \gg \sigma_d$, dependence of $\sigma(x)$ on metallic side of MIT obeys the relationship of

$$\sigma(x) = \sigma_d(x_C - x)^{-q} \quad (3)$$

where the critical index q is close to 1. The 3D percolative models for the binary mixtures give $t \approx$ 1.6–1.9 and $s \approx$ 0.5–0.62 [2, 30].

Figure 2b shows that by approaching x_C from metallic side (curve 1 in Fig. 2b) and from dielectric side (curve 2

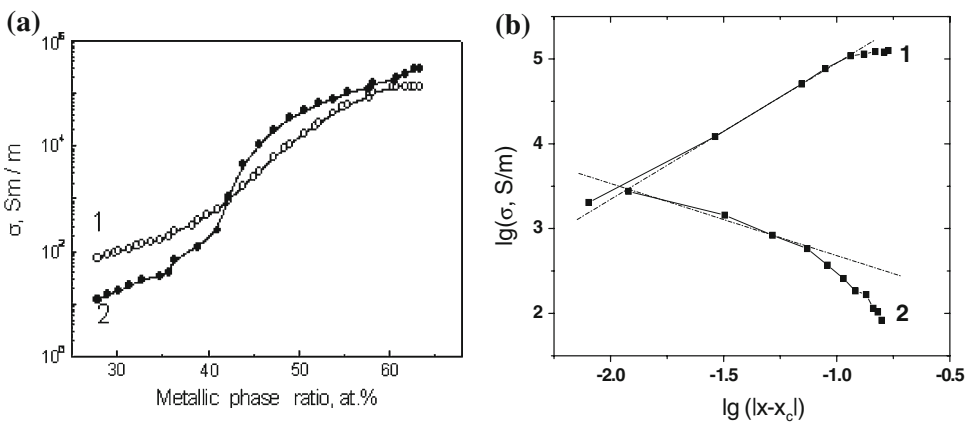

Fig. 2 Dependences of the real part of AC conductance σ at room temperature on volume ratio x of the metallic phase in the nanocomposites studied before (1) and after (2) 30 min vacuum annealing at temperature of 650 K (**a**) and in double logarithmic coordinates for the curve 1 (**b**). Dashed straight lines correspond to the approximations by relations 1 and 3

in Fig. 2b) the experimental dependences $\sigma(x)$ practically followed the relations 1 and 3 with the approximating parameters $t \approx 1.6$, $\sigma_m \approx 3.16 \times 10^6$ S/m, $q \approx 0.9$, and $\sigma_d \approx 63.9$ S/m. Substituting these parameters in relation 2 with $s \approx 0.62$ we find that $\sigma(x_C) \approx 3.85 \times 10^3$ S/m. The position of this value in Fig. 2a just corresponds to the value $x_C \approx 42$ at.% where curves 1 and 2 are crossed.

Frequency and temperature dependencies of real part conductance $\sigma(f,T)$ of the composites sputtered on non-water-cooled substrate for different metal alloy contents x are presented in the Fig. 3 as 3D pictures.

Comparative analysis of $\sigma_{real}(T,f)$ behavior displays the percolation threshold position for the studied composites between 41 and 44 at.% as illustrated in the 3D σ_{real}–T–f surface shape in Fig. 3c and d. In particular, a sign change of $d\sigma/dT$ can be seen from positive (activating regime of conductance) at $x < 41$ at.% to negative (metallic regime) for $x > 44$ at.% that confirms the value of $x_C \approx 42$ at.% following from Fig. 2a. Moreover, a transition of $\sigma_{real}(f)$ can be seen at $T = \text{const}$ from frequency-independent behavior below the x_C to a strong frequency dependence at $f > 50$ kHz beyond the x_C.

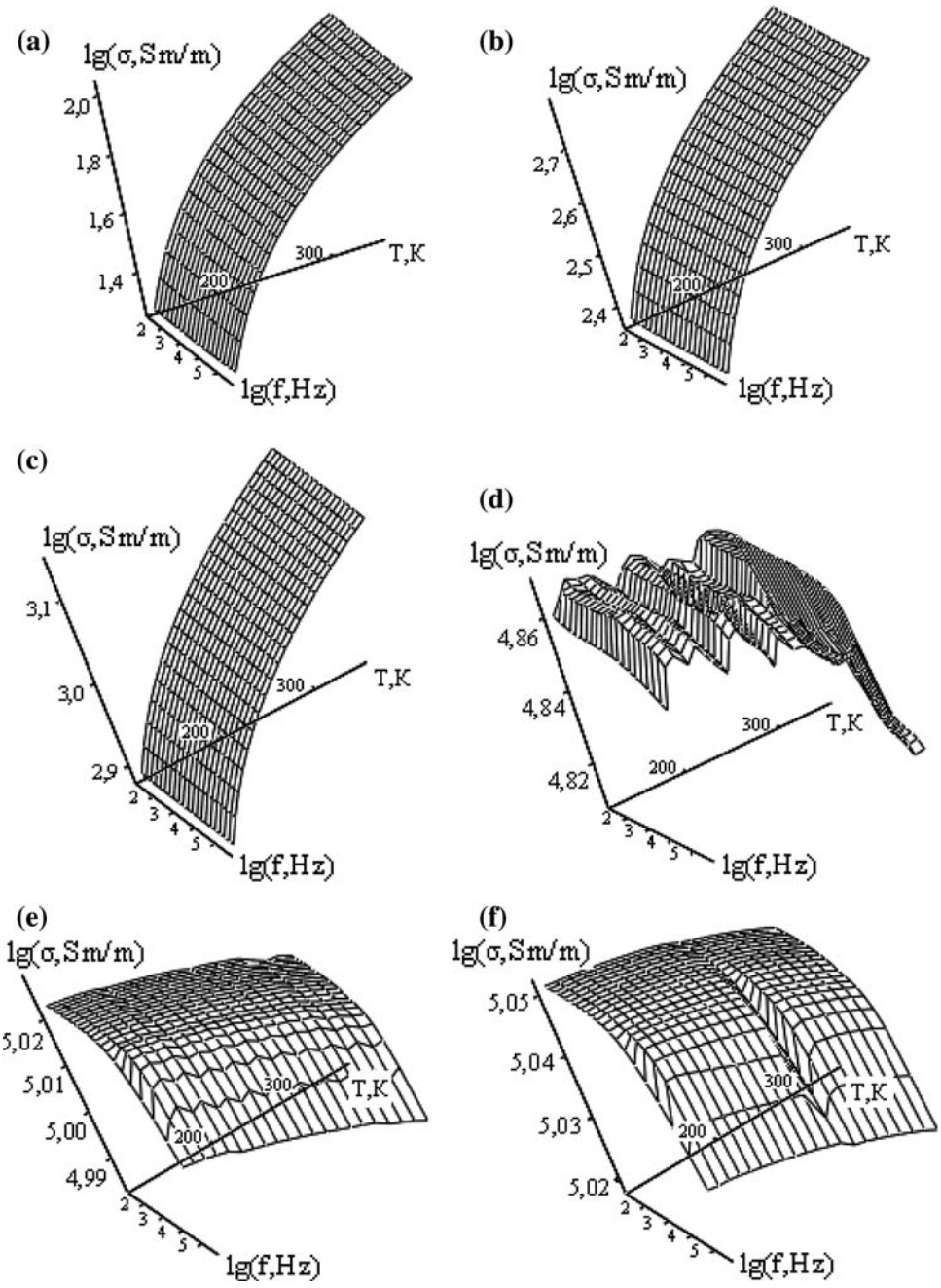

Fig. 3 Frequency and temperature dependencies of real part of conductance $\sigma(f,T)$ of the composites with different concentrations of metallic phase: $x = 31$ at.% (**a**); 39 at.% (**b**); 42 at.% (**c**); 48 at.% (**d**); 54 at.% (**e**); 64 at.% (**f**)

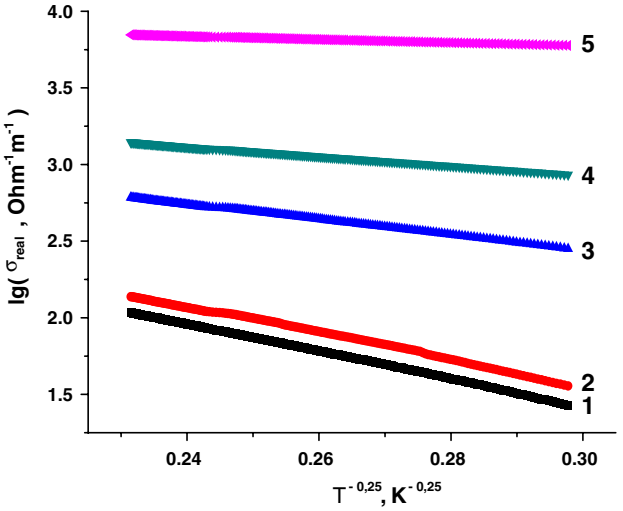

Fig. 4 Approximations of $\sigma_{real}(T)$ dependencies by Mott law for $f = 10$ kHz and different metal-to-dielectric ratios: 1—31 at.%; 2—33 at.%; 3—39 at.%; 4—42 at.%; 5—48 at.%; 6—54 at.%; 7—59 at.%; 8—64 at.%

To investigate in more detail the AC conductance mechanisms in the composites studied, the sections of $\sigma_{real}(T,f)$ dependences for constant frequencies can be used and the corresponding $\sigma_{real}(T)$ curves for $f < 10$ kHz and different x values are shown in Fig. 4. Inasmuch as the $\sigma_{real}(T)$ curves, Fig. 3b–c, are characterized by $(d\sigma/dT) > 0$ below the percolation threshold we have rebuilt them in the form of $\ln \sigma_{real}(T) - (1/T)^n$ with $n = 0.25$ and 0.5. The previous papers [31] showed that the DC conductance temperature dependence of the nanocomposites $(Fe_{0.45}Co_{0.45}Zr_{0.10})_x(Al_2O_3)_{1-x}$ sputtered on water-cooled substrate obeyed the relationship of

$$\sigma(T) = \sigma_o \exp\left[-\left(\frac{T_o}{T}\right)^{-n}\right] \tag{4}$$

which corresponds to hopping of electrons by localized states in the dielectric matrix. The exponent n in 4 is equal to 0.25 for Mott model of electrons hopping by localized states around Fermi level [32] and to 0.5 for Shklovski–Efros model [30] for hopping of electrons over the Coulomb gap in the density of localized states at Fermi level. The conducted analysis of approximation errors by fitting of $\sigma_{real}(T)$ by these two models made it possible to assert that the Mott law ($n \approx 0.25$) is valid in the whole temperature region. Moreover, comparing analysis of the curves presented in Fig. 4 with the earlier results [22–24, 31] for DC/AC conductance of the nanocomposites $(Fe_{0.45}Co_{0.45}Zr_{0.10})_x(Al_2O_3)_{1-x}$ deposited on water-cooled substrate results in some differences and some analogies in the behavior of $\sigma_{real}(T)$ and $\sigma_{DC}(T)$ dependencies. Firstly, the character of $\sigma_{real}(T)$ in Fig. 4 is qualitatively close to $\sigma_{DC}(T)$ in [31] pointing out to the hopping mechanism of carrier transport. However, as compared to $\sigma_{DC}(T)$, where sharp change of T_o in formula 4 at $T \approx 110$ K [31] was observed, curves 1–4 of Fig. 4 show only sole T_o for the whole temperature region 80–340 K. It means that, as compared with the previous results, higher temperature of the films deposition resulted in the formation of only one system of percolating routes for carrier transport in the studied temperature range.

One more difference between the two types of the studied films is related to the different behavior of $\sigma_{real}(T)$ in Fig. 3d–f and curves 5, 7, and 8 in Fig. 4 and $\sigma_{DC}(T)$ in [31] beyond the percolation threshold. The $\sigma_{DC}(T)$ in [31] at $x > x_C$ also followed the formula 4 with $n = 0.25$ but with much lower values of T_o than for $x < x_C$ whereas $\sigma_{real}(T)$ dependences changed sign of $(d\sigma/dT)$ at $x > x_C$ directly indicating the metallic regime of carrier transport.

The temperature dependences of nanocomposite conductivity allowed to estimate principally the changes in the localized state density $N(E_F)$ and/or localized wave function damping length a in alumina depending on the metallic phase content. For this procedure we used the semiempirical Kirkpatrick formula [33]

$$\sigma = 0.0217\left(\frac{C_1}{a}\right)\left(\frac{T_o}{T}\right)^{0,.35}\exp\left[-\left(\frac{T_o}{T}\right)^{0,25}\right], \tag{5}$$

with

$$T_o = \frac{60}{\pi k_B N(E_F) a^3}, \quad C_1 = \left(\frac{E_1^2}{\pi^4 d s^5 \hbar^4}\right)\cdot\left(\frac{e^3}{6\pi\varepsilon\varepsilon_0 a}\right)^2, \tag{6}$$

and Austin-Mott relation [34]

$$\sigma_{AC} = C_2 e^2 k_B T f N(E_F)^2 a^5 \ln^4\left(\frac{\nu_{ph}}{2\pi f}\right). \tag{7}$$

Here C_1 and C_2 are model constants, f—measurement frequency, a—the localized wave function damping length, e—the electron charge, k_B—Boltzmann constant. The parameters values used in this relations for Al_2O_3 were: $\nu_{ph} \approx 2 \times 10^{13}$ Hz—phonon frequency, $\theta_D \approx 1042$ K—Debye characteristic temperature, $E_1 \approx 10$ eV—deformational potential, $d \approx 3.97$ g/cm^3—density, $s \approx 3 \times 10^3$ cm/s—sound velocity, $\varepsilon\varepsilon_0 \approx 10$—dielectric constant.

Calculated values of $N(E_F)$ and a are presented in Table 1. Moreover, the dependency of $N(E_F)$ on metal-to-dielectric volume ratios calculated from the semiempirical Kirkpatrick formulas 5, 6 gives the same tendency as in [29] estimated from DC conductivity results, i.e., density of localized states at Fermi level increases by one order as x increases.

However, the $N(E_F)$ values in this case are about 2–3 orders of magnitude less than that in [29]. Note that $N(E_F)$ in [29] were calculated from Mott relation (see, [6]) with a

Table 1 Effective values of $N(E_F)$ and a on dielectric side of MIT in the studied nanocomposites

x (at.%)	T_o (K)	Calculations by formulas 5, 6 using experimental values of T_o and σ_o			Calculations by formula 7 with a values taken from 5th column
		σ_o (S/m)	$N(E_F)$ (eV^{-1} cm^{-3})	a (nm)	$N(E_0)$ (eV^{-1} cm^{-3})
31	510000	4100	2.7×10^{17}	11.9	1.5×10^{20}
33	470000	4500	3.1×10^{17}	11.2	1.7×10^{20}
39	94000	4900	8.2×10^{17}	11.2	3.7×10^{20}
42	30000	6100	2.1×10^{18}	10.4	5.7×10^{20}

questionable assumption that the electron wave-function localization length a is close to 0.8 nm but in this paper a values about 11 nm were extracted directly from Kirkpatrick formulas 5, 6 without any additional assumptions. Substituting this value into formula 7 with $T = 300$ K and $f = 10$ kHz the last column of Table 1 shows a similar tendency—the $N(E_F)$ increase as x increase but weakly expressed. Therefore, numerical estimations of the $N(E_F)$ and a values should be considered only as the tendency of their changes depending on the composition. This tendency is attributed here to the increase of the interface metal-dielectric areas with the x growth. Indeed, a number of localized states, occurring at the phase interface due to their incoherence, should be increased with the increase of metallic nanoparticles concentration.

In summary we need to do one remark in connection with the conducted estimations. A complicated phase structure of the studied composites resulted in the creation of large-scale potential relief in the films due to the presence of the random potential barriers impeded the movement of carriers by dielectric matrix between the conducting metallic nanoparticles. This should cause the formation of very complicated system of the current-conducting routes for the samples (especially on the dielectric side of MIT, with $x < x_C$) that are highly inhomogeneously distributed by the film depth and plane of the films. This circumstance allowed the use of the percolation theory to explain carrier transport in metal-dielectric composites. This implied that the real length of percolating routes, especially at low temperatures, became much longer and thinner (with smaller cross-sections) than the actual sample size. At higher temperatures, some of barriers (dielectric strata) became transparent for carriers and these percolating routes became closer to the sample length and wider (with greater cross sections). It means that real values of cross section-to-length factor (S/l) of the percolating routes are changed with temperature and do not coincide with the ratio of sample cross section to its length which was used in the present estimations of conductivity. In other words, exact estimation of the cross sections and lengths of the current-conducting regions in each sample at a precise temperature becomes impossible.

Conclusion

Results of this work and analysis of the previous papers and literature have shown that composition and deposition conditions have a very strong influence on carrier transport of nanocomposite films containing CoFeZr nanoparticles embedded into amorphous alumina matrix. In particular, for the samples deposited at the higher temperatures (~ 100 °C) the following features were observed:

1. Low frequency ($f \leq 5$ kHz) real part of AC conductance at the temperatures of 80–340 K for the studied samples are described by Mott law that are characteristic of the thermally activated tunneling (hopping) mechanisms of the carrier transport by the localized states near Fermi level in the studied regions of temperatures and concentrations of the metallic phase. However, in contrast to the films deposited at lower temperatures (on water-cooled substrate), in the studied samples $\sigma_{real}(T)$ dependencies are described by Mott law (4) with sole parameter T_o for the whole temperature region 80–340 K.
2. The dependence of real part of AC conductance on the fraction of metallic phase $\sigma_{real}(x)$ principally coincided with the corresponding behavior of DC conductance but accompanied by abrupt change of $(d\sigma_{real}/dT)$ sign from negative to positive when crossing the percolation threshold confirming transition from activational to metallic regime of conductance.
3. It was shown that $\sigma_{real}(T)$ dependencies satisfactorily follow the known relations of 3D percolative models with critical indexes $t \approx 1.6$, $q \approx 0.9$, and $s = 0.62$.
4. The numerical estimations of the density of localized states $N(E_F)$ displayed a tendency to be increased as x increased and the electron wave-function localization length a was about 11 nm.

Acknowledgement The author wishes to thank Belarusian State University especially Prof. A. Fedotov for allowing him to do this work during his devoted summer vacations for the last several years and also Prof. Yu. Kalinin from Voronezh State Technical University for presentation of the samples.

References

1. Salz D, Wark M, Baalmann A, Simon U, Jaeger N (2002) Phys Chem Chem Phys 4:2438
2. Stauffer D, Aharony A (1992) Introduction to percolation theory. Taylor and Francis, London
3. Boltcher CJF, Bordewijk P (1978) Theory of electric polarization, vol I & II, 2nd edn. Elsevier, New York
4. McCrum NG, Readond BE, Williams G (1967) Anelastic and dielectric effects in polymeric solids. Wiley, New York
5. Wong J, Angell CA (1976) Glasses: structure by spectroscopy. Marcel Dekker, New York
6. Mott NF, Davis EA (1971) Electronic processes in non crystalline materials, 2nd edn. Oxford University, New York
7. Pollak M, Geballe TH (1961) Phys Rev 122:1742
8. Li W, Sun Y, Sullivan CR (2005) IEEE Trans Magn 41:3283
9. Sullivan CR, Prabhakaran S, Dhagat P, Sun Y (2003) Trans Magn Soc Jpn 3:126
10. Dhagat P, Prabhakaran S, Sullivan CR (2004) IEEE Trans Magn 40:2008
11. Saad AM, Mazanik AV, Kalinin YuE, Fedotova JA, Fedotov AK, Wrotek S, Sitnikov AV, Svito IA (2004) Rev Adv Mater Sci 8:34
12. Dieny B, Speriosu VS, Metin S et al (1991) J Appl Phys 60:4774
13. Wang ZJ, Mitsudo S, Watanable J (1997) J Magn Magn Mater 176:127
14. Jonker B et al (2000) Phys Rev B 62:8180
15. Kobayashi N, Ohnuma S, Masumoto T, Fujimori H (2001) J Appl Phys 90:4159
16. Grunberg P (2001) J Phys Condens Matter 13:7691
17. Schmidt G, Molenkamp LW (2002) Semicond Sci Technol 17:310
18. Nishimura N, Hirai T, Koganei A et al (2002) J Appl Phys 91:5246
19. Almokhtar M, Mibu K, Shinjo T (2002) Phys Rev B 66:134401
20. Zaharko O, Oppeneer PM et al (2002) Phys Rev B 66:134406
21. Kalaev VA, Kalinin YuE, Necaev VN, Sitnikov AV (2003) Bull Voronezh State Tech Univ Mater Sci 13:38
22. Saad AM, Fedotov AK, Fedotova JA, Svito IA, Andrievsky BV, Kalinin YuE, Fedotova VV, Malyunina-Bronskaya V, Patryn AA, Mazanik AV, Sitnikov AV (2006) Phys Status Solidi C 3:1283
23. Saad AM, Fedotov AK, Svito IA, Mazanik AV, Andrievski BV, Patryn AA, Kalinin YuE, Sitnikov AV (2006) Prog Solid State Chem 14:139
24. Saad AM, Fedotov AK, Svito IA, Fedotova JA, Andrievsky BV, Kalinin YuE, Patryn AA, Fedotova VV, Malyutina-Bronskaya V, Mazanik AV, Sitnikov AV (2006) J Alloys Compd 423:176
25. Huang JCA, Hsu CY (2004) Appl Phys Lett 24:85
26. MacDonald JR (2005) Solid State Ionics 176:1961
27. Fedotova J, Kalinin Yu, Fedotov A, Sitnikov A, Svito I, Zalesskij A, Jablonska A (2005) Hyperfine Interact 165:127
28. Grimmet G (1999) Percolation. Springer-Verlag, Berlin, p 444
29. Kalinin YuE, Remizov AN, Sitnikov AV (2004) Phys Solid State 46:2146
30. Efros AL, Shklovski BI (1976) Phys Status Solidi B 76:475
31. Saad AM, Andrievsky B, Fedotov A, Fedotova J, Figielski T, Kalinin Yu, Malyutina-Bronskaya V, Mazanik A, Patryn A, Sitnikov A, Svito IA (2005) In: Podor B, Horvath ZsJ, Basa P (eds) Proceedings of the 1st international workshop on semiconductor nanocrystals (SEMINANO), Budapest, Hungary, 10–12 Sept 2005, p 321
32. Mott NF, Devis EA (1979) Electron processes in noncrystalline materials. Clarendon Press, Oxford
33. Yasuda K, Yoshida A, Arizumi T (1977) Phys Status Solidi A 41:k181
34. Austin IG, Mott NF (1969) Adv Phys 18:41